RSC Applied Interfaces

ROYAL SOCIETY OF CHEMISTRY

PAPER

View Article Online
View Journal | View Issue

Check for updates

Cite this: *RSC Appl. Interfaces*, 2025, 2, 1395

Investigation of the chemical structure of fluorinated diazonium salts on the electrografting behavior and thin film properties†

Rébecca Bazin, Jocelyne Leroy, Mélanie François and Bruno Jousselme *

Received 14th April 2025,
Accepted 26th June 2025

DOI: 10.1039/d5lf00106d

rsc.li/RSCApplInter

Many industrial and commercial applications require hydrophobic or super oleophobic surfaces. Fluorinated compounds provide surfaces with excellent hydrophobicity, but for environmental reasons, it is crucial to minimize their use. In this context, the electrografting of fluorinated diazonium salts enables the deposition of very thin films. This work investigates the impact of the chemical structure (different position or/and chain length) of these diazonium salts on the growth of the resulting film. Ultimately, the main objective is to understand the grafting mechanism in order to precisely achieve the desired properties. This study demonstrates that the chemical structure of diazonium salts greatly influences the film growth process, and, consequently its physical characteristics, such as compactness and hydrophobicity.

1. Introduction

Since the 1950s, per- and poly-fluoroalkyl substances (PFAS) have been extensively used in various industrial and commercial applications due to their anti-adhesive, water-resistant, and heat-resistant properties. These substances have been incorporated into numerous products, including non-stick coatings (*e.g.*, frying pans), water-resistant textiles, and grease- and moisture-resistant food packaging.[1] More than a megaton of PFAS is produced every year worldwide, and thousands of tons end up in everyday consumer products.[2] Due to the strength of the carbon-fluorine bonds, these substances are very persistent in the environment, which has recently led to stringent restrictions on their use.

Their widespread use has resulted in significant environmental contamination, air pollution and health risks.[3] Consequently, fluorinated compounds are now frequently identified among emerging environmental contaminants, especially as persistent organic pollutants (POPs).[4] This underscores the need for effective control measures and minimization of deposition on substrates, in order to reduce the overall quantities required and mitigate their environmental impact. Today, several techniques are available to pattern surfaces with fluorinated agents: chemical vapor deposition (CVD),[5] electrospinning,[6] atmospheric pressure plasma jets (APPJ),[7] and physical vapor deposition (PVD), such as plasma sputtering.[8] These methods allow the deposition of films ranging from a few tens of nanometers (PVD, electrospinning) to a few tens of micrometers (plasma sputtering, APPJ). Over the past decade, electrografting has emerged as a powerful method for surface modification and organic grafting.[9] It enables the easy formation of nanometer sized thin organic films that are covalently bonded to conductive substrates (carbon or metals) or semiconductors. The chemical grafting of diazonium salts can also be performed on insulating materials.[10] Various substituents, including fluorine (F) atoms, trifluoromethyl (CF_3),[11,12] or perfluoroalkyl,[13] can be introduced into the benzene ring of diazoniums, making this deposition method valuable for numerous applications, such as electronics, where Fluorinated organic ultrathin films are used to form effective gate dielectrics in MoS_2 transistors.[13]

While obtaining a single monolayer by electrografting is theoretically possible, it requires limiting parallel polymerization processes. Several methods have been investigated for this purpose. The first, developed by Daasbjerg *et al.* in 2007,[14,15] is based on the formation-deformation approach. A multilayer structure is created with weakly bonded layers that can be easily broken using an ultrasound bath, resulting in a stable monolayer. In 2009, Podvorica *et al.*[16] introduced an alternative method to control film deposition through steric effects. By manipulating the position and/or the length of the substituent chains, they achieved different degrees of grafting, resulting in different film thicknesses. In 2013, Breton *et al.*[17] explored the use of a radical scavenger, 2,2-diphenyl-1-picrylhydrazyl, to control the number of diazonium salts in the diffusion zone. This

CEA, CNRS, NIMBE, LICSEN, Université Paris-Saclay, Gif-sur-Yvette, 91191, France. E-mail: bruno.jousselme@cea.fr

† Electronic supplementary information (ESI) available. See DOI: https://doi.org/10.1039/d5lf00106d

approach effectively limits the quantity of diazonium salts that reach the surface, allowing control of the final thickness. In 2018, the same author demonstrated that oxygen can also be used as a radical scavenger.[12]

To obtain a film with minimal fluorinated groups, the steric effect method was investigated. A variety of fluorinated molecules with different substituents (Fig. 1) were investigated to assess their influence during the electrografting process. More precisely, the objective of this study is twofold: (1) to explore the application of electrografting technique for depositing thin film of various fluorinated molecules on gold and glassy carbon electrodes; and, (2) to elucidate the processes that impact the growth and compactness using a variety of techniques including Electrochemical Quartz Crystal Microbalance (EQCM), Cyclic voltammetry (CV) and X-ray Photoelectron Spectroscopy (XPS). Few studies have demonstrated the successful electrografting of fluorinated diazonium salts onto substrates such as carbon and gold.[13] However, here we will focus on investigating the growth of the films and the resulting properties based on the different geometries of the diazonium salts.

2. Materials and methods

Chemical and salt synthesis

All starting amino compounds were purchased from ABCR or Sigma Aldrich. Nitrosium tetrafluoroborate was obtained from Aldrich and used as received. NMR spectra were recorded with a Bruker ADVANCE DRX 400 spectrometer (400 MHz). Chemical shifts (δ) are reported in ppm relative to tetramethylsilane (TMS). Infrared (IR) spectra were acquired with a Bruker Vertex 70 spectrometer (resolution 2 cm^{-1}, 24 scans collected, MCT detector) equipped with a Pike Miracle plate for ATR.

The fluorinated diazonium salts were synthesized according to the literature.[13] Briefly, the amino compound was dissolved in a minimum amount of acetonitrile (ACN) at −40 °C. A slight molar excess (*e.g.*, 1.2 equivalents) of solid nitrosium tetrafluoroborate ($NOBF_4$) was added all at once. The reaction mixture was stirred for 15 minutes at −40 °C. Then, the mixture was poured into cold diethyl ether and the precipitate formed was filtered off, washed with cold diethyl ether, and then dried under vacuum to give the diazonium salt.

All the infrared (Fig. S1) and NMR (Fig. S2–S5) spectra and data are in the ESI.†

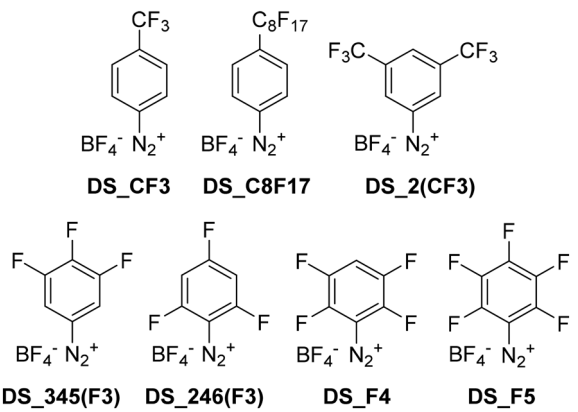

Fig. 1 Chemical structures of fluorinated diazonium salts.

Substrates preparation

Gold surfaces for XPS analysis were prepared by vacuum evaporation of pure gold onto 1 cm × 6 cm glass substrates at room temperature. Prior to evaporation, the glass substrates were cleaned by sequential sonication in deionized (DI) water with Decon, acetone, isopropanol and dryed with N_2. A 5 nm chromium sublayer was first deposited in a Balzers BAK 600 evaporator to enhance gold adhesion to the substrate. Then, 90 nm of gold was evaporated under a residual pressure of 10^{-7} bar.

Glassy carbon (LGCE Glassy Carbon) and gold electrodes, both with a diameter of 3 mm, were purchased from ALS. As cleaning procedure, the electrodes were polished with QATM diamond polishing pads with grit sizes of 3 μm and 1 μm. After each polishing step, the electrodes were thoroughly rinsed with DI water.

Electrografting procedure

Electrochemical experiments were performed using a Biologic SP300 VSP potentiostat, monitored and controlled *via* EC-Lab software. All potentials are reported *versus* saturated Ag/AgCl reference electrode in aqueous medium and $Ag/AgNO_3$ (10 mM) in organic medium. Platinum gauze was used as the counter electrode. The modification of the electrodes was performed by Cyclic voltammetry (CV) at a scan rate of 100 mV s^{-1} in an ACN solution containing 0.1 M tetrabutylammonium hexafluorophosphate (n-Bu_4NPF_6) and 1 mM diazonium salts. Following the deposition, the electrodes were immersed in ACN for 10 minutes to remove the electrolyte within the film.

Characterization methods

EQCM measurements using a Seiko-EG&G QCM922 microbalance (Princeton Applied Research) were employed to monitor *in situ* the grafting process by detecting real-time mass changes. For that experiment CV were performed between [0.3; −1] V *vs.* Ag/Ag^+ in ACN/0.1 M n-Bu_4NPF_6 electrolyte and 1 mM diazonium salts. The microbalance utilizes a gold resonator (Standard Finish, 0.6 μm roughness) from HTDS. After deposition, the chemical composition of the grafted film was characterized by XPS on a Kratos Axis Ultra DLD spectrometer (Kratos Analytical Ltd., Manchester, UK) using a high resolution monochromatic Al-Kα line X-ray source at 1486.6 eV. Fixed analyzer pass energy of 40 eV was used for core level scans. A survey spectrum and core-level spectra of C_{1s}, Au_{4f} and F_{1s} regions were systematically recorded. The data treatment was performed with the

CasaXPS software. The measurements were carried out on the same surface area of 300 × 700 μm^2. The core level was referenced to the F_{1s} binding energy at 689.0 eV to study carbon-fluorine bonds and to the Au_{4f} binding energy at 84.0 eV to study gold. The elemental concentration ratios were calculated using normalized peak. To characterize the electrochemical behavior of the modified electrodes, CV were performed between [0; 0.6] V *vs.* Ag/AgCl in 5 mM $Fe(CN)_6^{3-/4-}$ + 0.5 M Li_2SO_4. In addition, contact angle measurements (Dataphysics, OCA 15 EC) were used to characterize the degree of hydrophilicity of the grafted layer on both glassy carbon and gold electrodes.

3. Results and discussion

Seven fluorinated aryldiazonium salts (chemical structures represented in Fig. 1) were selected based on specific criteria. In general, multilayer formation during diazonium electrografting is favored when the *meta* and *para* positions on the aryl ring are available (C–H Bond) for further radical attack. This is because once the initial aryl layer is grafted onto the surface, the aryl radicals generated during continued electrochemical reduction can react with free positions (especially *meta* and *para*) on the previously grafted layer, promoting film growth and leading to multilayer structures. This behavior has been reviewed by Pinson and Podvorica.[18] Therefore, the first criterion focuses on evaluating the steric hindrance of the substitution sites on the aromatic ring. It is expected that when the *para* or *meta* positions are available (as in **DS_F4**, **DS_246(F3)**) multilayer formation would occur. In contrast, if no positions are available or only the *ortho* positions (as in **DS_F5**, **DS_345(F3)**) are accessible, monolayer formation should be favored. However, Pinson and Podvorica[16] previously published the formation of a thin film from **DS_F5**, suggesting some complexity in the grafting behavior. The second criterion proposes to evaluate the impact of the length of the substituent with **DS_CF3** and **DS_C8F17**. It is expected that longer chains will result in thicker grafted film, although the exact outcome depends on the chains length. Breton and Gautier,[19] inspired by the work of Tanaka and Sawaguchi,[20] demonstrated that spontaneous grafting of a diazonium salt bearing a long aryl chain ($DC_{12}Fc$) produce a monolayer. The presence of a long alkyl chain prevents electrons tunneling through the first grafted organic layer, thereby promoting the formation of a uniform monolayer. Finally, these two properties, steric hindrance of the substitution sites and chain length were combined in **DS_2(CF3)**. The electrografting of this last diazonium salt, previously described by Pinson and Podvorica[16] proved efficient for multilayer formation. This contrast with diazonium salts bearing bulky substituents at the *ortho* position, which inhibit surface functionalization.

The diazonium salts were synthesized from commercial amino compounds using nitrosium tetrafluoroborate. This method was chosen because both $NOBF_4$ and the fluorinated anilines are only soluble in organic solvents. The non-nucleophilic nature of the BF_4^- counterion allows for the stable isolation of the diazonium salts and ensures good solubility in organic media, which is essential for electrografting.

The diazonium functional group was confirmed through infrared spectroscopy, which revealed a specific peak at 2250 cm^{-1} corresponding to the N≡N bending vibration. In addition, Nuclear Magnetic Resonance (NMR) spectroscopy was employed for further verification (see ESI†).

The following sections study the impact of the steric effects and chain length on the film growth and quality of the electrografting process on glassy carbon and gold substrates. We will therefore quantify both the steric effects and chain length impacts on the main grafting steps: (i) the reduction of diazonium salts at the electrode surface, (ii) the formation of covalent bond, (iii) the surface passivation, and, (iv) the film growth.

Influence of steric effects on growth and quality of the electrografting on gold and GC substrates

Diazonium salts were dissolved in *n*-NBu_4PF_6/ACN electrolyte and electrografted using cyclic voltamperometry at a scan rate of 100 mV s^{-1}. Potentials are reported *versus* Ag/Ag^+ reference electrode and platinum gauze was used as counter electrode. Fig. 2 shows the voltammograms obtained for the **DS_F4**, **DS_246(F3)**, **DS_345(F3)** and **DS_F5** salts, during the grafting on both GC and gold surfaces. For all of them, during the first reduction cycle, one peak is observed in the range of 0.2 V to −0.4 V *vs.* Ag/Ag^+ reference electrode (Table 1), corresponding to the reduction of the diazonium function. The presence of two peaks in the CVs on gold electrode was attributed by Benedetto *et al.*[21] to electrografting occuring on different crystallographic facets of the gold surface. Then, as the number of cycle progresses, the peak intensity diminishes, indicating a decrease in electronic transfer. This decrease suggests that the film is becoming insulating, reflecting the successful functionalization of the surface throughout the cycling process. It is well-established that the phenomenon responsible for the attenuation of a wave is the formation of an organic layer that adheres to the electrode.[18]

The voltammograms in Fig. 2 show two different grafting profiles. One, observed in the curves corresponding to the **DS_F4** and **DS_246(F3)** salts, is characterized by an irreversible wave present in the first cycle which disappears in the second cycle. The electron transfer is therefore blocked, indicating the effective fast formation of a passivating layer. Instead, for the **DS_345(F3)** and **DS_F5** salts, the first wave diminishes over successive cycles until it finally disappears, indicating the formation of passivating layer. In addition, the current densities are higher for the curves (**DS_345(F3)** and **DS_F5** salts) that do not exhibit rapid

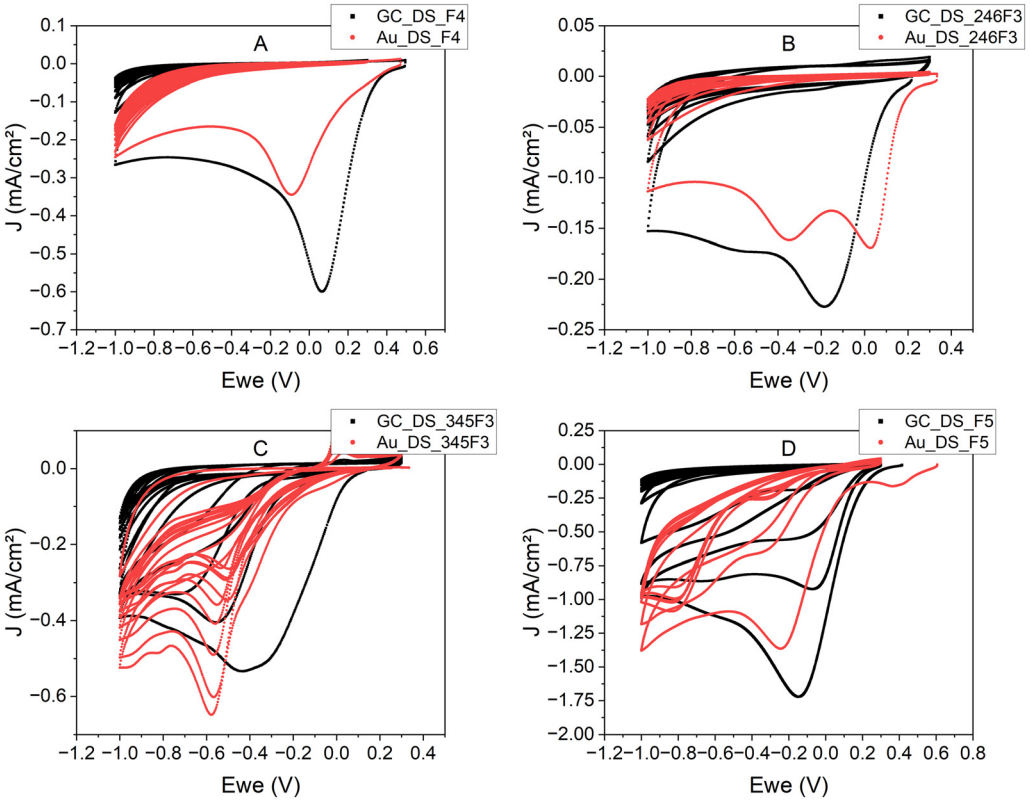

Fig. 2 Cyclic voltammograms recorded at a sweep rate of 100 mV s^{-1} on GC (black) and gold (red) electrodes in 1 mM solutions of 4 salts: **DS_F4** (A), **DS_246(F3)** (B), **DS_345(F3)** (C), and, **DS_F5** (D). The salts were dissolved in an *n*-NBu_4PF_6/ACN electrolyte. All potentials are reported *versus* an Ag/Ag^+ reference electrode, with a platinum gauze as counter electrode.

passivation. The grafting process is therefore influenced by the position of the fluorine atoms on the aromatic ring. When the C–H are available in *para* position (**DS_F4**) or *meta* positions (**DS_246(F3)**), the formation of multilayers is favored compared to the salts where the aromatic ring lacks hydrogen or has hydrogens in *ortho* positions, as for **DS_F5** and **DS_345(F3)**, respectively. However, for the latter two salts it is even more unusual to obtain the formation of multilayers, as shown by the formation of thin film passivating film on the carbon electrode (black curves on Fig. 2C and D). Two hypotheses can be drawn to explain this grafting behavior: the layer is simply physisorbed onto the surface, or, the growth of a multilayer film induces the release of a fluorine atom from the aromatic ring.

To determine whether the organic layer is physisorbed on the surface, the electrografted carbon electrodes were immersed in *N*,*N*-dimethylformamide (DMF) and sonicated in an ultrasonic bath for 2 minutes. Then the electrodes were characterized using CV in a 5 mM $Fe(CN)_6^{3-/4-}$ solution in 0.5 M Li_2SO_4. It is worth noting that various solvents such as dichloromethane, toluene, DMSO and DMA were tested and the one that gave the best solubilization of the material was DMF.

Fig. 3 shows the redox response of Ferri/Ferro in 0.5 M Li_2SO_4 electrolyte. The black curve is the response for blank

Table 1 Potential, current density and ratio of current densities of first and second wave of CV for each diazonium salts

	Potential (at −0.1 mA cm^{-2}) (V *vs.* Ag/Ag^+)		Current density (maximum at reduction peak) (mA cm^{-2})		Peak density ratio (2nd/1st cycle)	
Surface	GC	Au	GC	Au	GC	Au
DS_F4	0.29	0.19	−0.60	−0.35	0.03	0.06
DS_F5	0.51	0.47	−1.71	−1.36	0.54	0.48
DS_246(F3)	0.11	0.18	−0.23	−0.16	0.09	0.03
DS_345(F3)	0.17	0.11	−0.53	−0.65	0.75	0.92
DS_CF3	−0.12	0.11	−1.19	−1.08	0.86	0.90
DS_2(CF3)	0.01	0.11	−0.80	−0.71	0.60	0.48
DS_C8F17	−0.26	−0.15	−0.18	−0.16	0.06	0.06

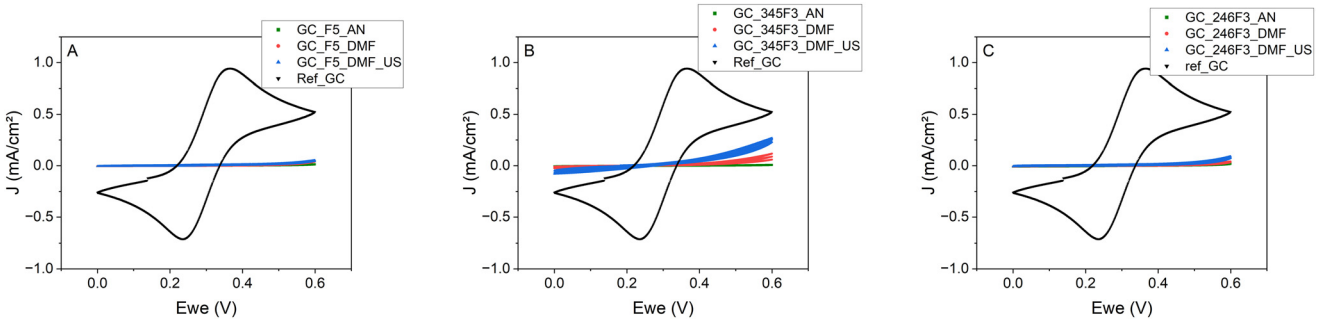

Fig. 3 Cyclic voltammograms at a scan rate of 50 mV s^{-1} for **DS_F5** (A), **DS_345(F3)** (B) and **DS_246(F3)** (C) grafting on GC electrodes before and after different baths in acetonitrile (red), DMF (green), and DMF + ultrasonic bath for 2 minutes (blue) in a 5 mM $Fe(CN)_6^{3-}/^{4-}$ solution.

GC electrodes (no grafted molecule) served as reference; in red, are the responses of the electrografted sample after 2 minutes in ACN. The green curves, which are not always clearly visible, show the response of the grafted electrode after 2 minutes in DMF: if the physisorbed species are dissolved, an increase in the redox response would be expected. Finally, the blue curves represent the response of the electrografted electrodes after ultrasonic stirring in DMF for 2 minutes. Results demonstrate that there is almost no difference in redox response for modified carbon electrodes, indicating that the organic compounds are predominantly chemisorbed. These results are thus consistent with the findings of Pinson and Podvorica,[16] which reported that the grafting of pentafluorobenzene diazonium salt involves the attack of a radical on a carbon atom bearing a fluorine and a formation of a multilayered film.

As summary, the first study shows also that there was no longer electron exchange between electrolyte and electrode, which is an indication that a passivating thin film was successfully created onto the surface. Considering that electron transfer depends on the thickness of the organic layer,[22] we conjecture that thick film formed following the departure of fluorine form the aromatic ring. Indeed a monolayer would not have produced a passivating film.

Influence of chain length on the dynamic and quality of the electrografting on gold and GC substrates

The influence of the substituent chain length on the electrografting process is now investigated using the same methodology. Fig. 4 shows the cyclic voltammograms obtained for the **DS_ C8F17**, **DS_CF3** and **DS_2(CF3)** salts during the grafting onto both GC and gold electrodes.

For the **DS_C8F17** salt, Fig. 4(A) shows irreversible waves on the first cycle, on both gold and carbon electrodes. During the second cycle, the almost zero current density for **DS_C8F17** indicates the formation of a highly passivating film. However, the CV obtained for the **DS_CF3** and **DS_2(CF3)** salts show significant differences when comparing GC and gold electrodes. On the gold electrode, the peak height remains almost constant after the first cycle, with only a slight decrease – a typical observation of difficult grafting. These CVs indicate an electron transfer process followed by reduction of the molecule's diazonium function, but they do not lead the grafting onto the electrode surface. On the carbon electrode, the redox signal of the **DS_CF3** and **DS_2(CF3)** derivatives decreases progressively – grafting appears to be slower. Moreover, for the two difficult-to-graft molecules, the current density is very high, leading to the formation of a greater number of reduced species. The behavior of **DS_2(CF3)** observed here appears to differ from

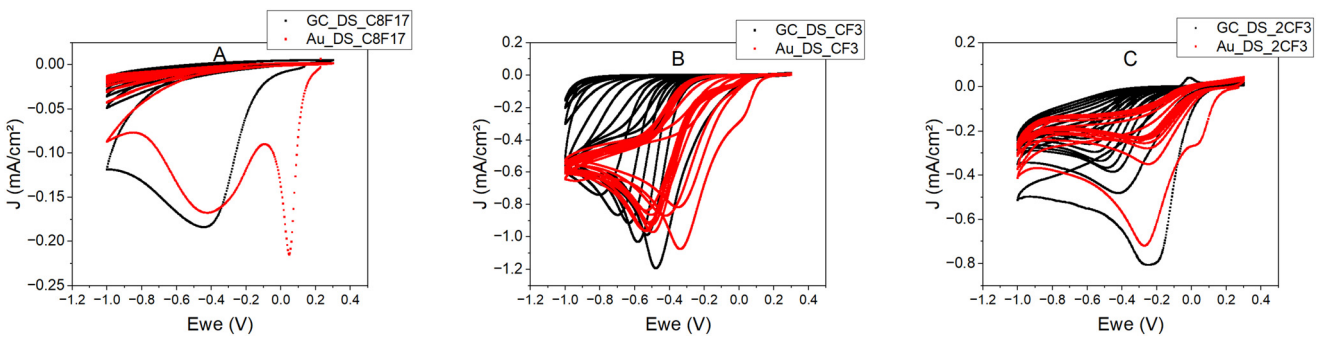

Fig. 4 Cyclic voltammograms recorded at a sweep rate of 100 mV s^{-1} on GC (black) and gold (red) electrodes in 1 mM solutions of **DS_ C8F17** (A), **DS_CF3** (B), and, **DS_2(CF3)** (C) salts. The salts were dissolved in a *n*-NBu_4PF_6/ACN electrolyte. All potentials are reported *versus* an Ag/Ag^+ reference electrode, with a platinum gauze as counter electrode.

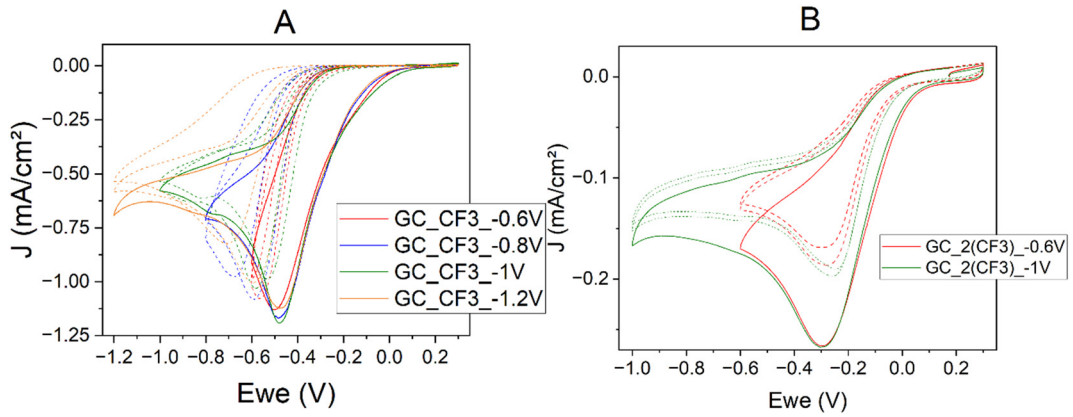

Fig. 5 Cyclic voltammograms recorded at a sweep rate of 100 mV s^{-1} on GC electrode in solutions of 1 mM of **DS_CF3** (A) and **DS_2(CF3)** (B) until different potential: −0.6 V (red), −0.8 V (blue), −1 V (green) and −1.2 V *vs.* Ag/Ag^+ (orange). The first cycle is shown as a solid line, while cycles 2 and 3 are represented with dashed lines.

previously reported results in the literature,[16] which described the formation of a thick multilayer film. However, it is difficult to compare and discuss these findings, as the CV curves were not reported.

The potential range swept during the electrochemical grafting can also play a role on the number of radicals formed. As previously published,[23] this must be taken into account when comparing two diazoniums with different functions. Therefore, a scan window study was carried out by varying the potentials from −0.6 V to −1.2 V *vs.* Ag/Ag^+, in 0.2 V increment for **DS_CF3** and **DS_2(CF3)** salts (Fig. 5). Extending the scan to −1.2 V results in the application of a more negative potential applied for a longer duration, which generates more radicals involves in thin film formation. However, extending the scan to more negative potentials did not yield significant changes in current density in the CV. The current density of the second wave and subsequent features remain largely unchanged regardless of the scan range. As consequence, the potential has no effect on the electrode passivation, unlike the molecule structure.

Influence of steric effect and chain length on film composition and thickness

Next, a more comprehensive study of the deposition of the different diazonium salts on gold electrodes was conducted using Electrochemical Quartz Crystal Microbalance (EQCM) and XPS to quantify the influence of the steric effect and chain length on the formed film thickness and chemical nature. Five diazonium salts were used for this section: **DS_C8F17**, **DS_F4**, and **DS_246(F3)** for which exhibited good grafting performance, and **DS_2(CF3)** and **DS_CF3** which showed limited grafting after the first cycle on gold.

The mass gain on the electrodes was measured by combining EQCM measurements with cyclic voltammetry. Supposing that the deposited organic layer is rigid and that no viscoelastic changes occur at the electrode interface, the relationship between the change in quartz frequency (Δf) and the mass change (Δm) can be described by the Sauerbrey equation:[24]

$$\Delta m = -\Delta f \times S \quad (1)$$

S is a sensitive factor characteristic of the quartz crystal equal to 1.09 ng Hz^{-1} in our case. Fig. 6 shows the temporal mass gain measured during the grafting of **DS_C8F17**, **DS_2(CF3)** and **DS_F4** salts.

Fig. 6 shows the grafting kinetics based on mass gain on the electrodes obtained from the EQCM measurements for the different diazonium salts. In Fig. 6, the mass gain of the gold-quartz electrode modified with **DS_F4** (green curve) shows a large increase in mass on the first scan, then a consistent mass increase (43.2 μg cm^{-2}) during the cycling indicating the formation of a multilayer film. In contrast, after a similar large increase on the first scan, the **DS_C8F17**

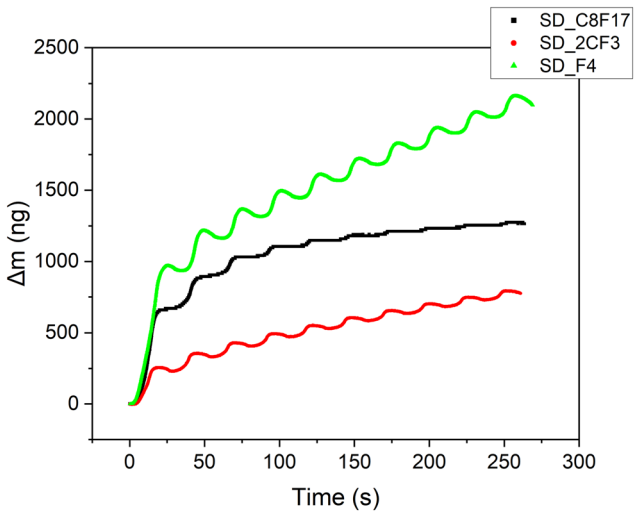

Fig. 6 Mass changes of the gold-quartz electrode (S = 5 mm^2) measured by EQCM during the electrochemical grafting (10 cycles) of 1 mM solutions of **DS_C8F17**, **DS_2(CF3)** and **DS_F4** salts.

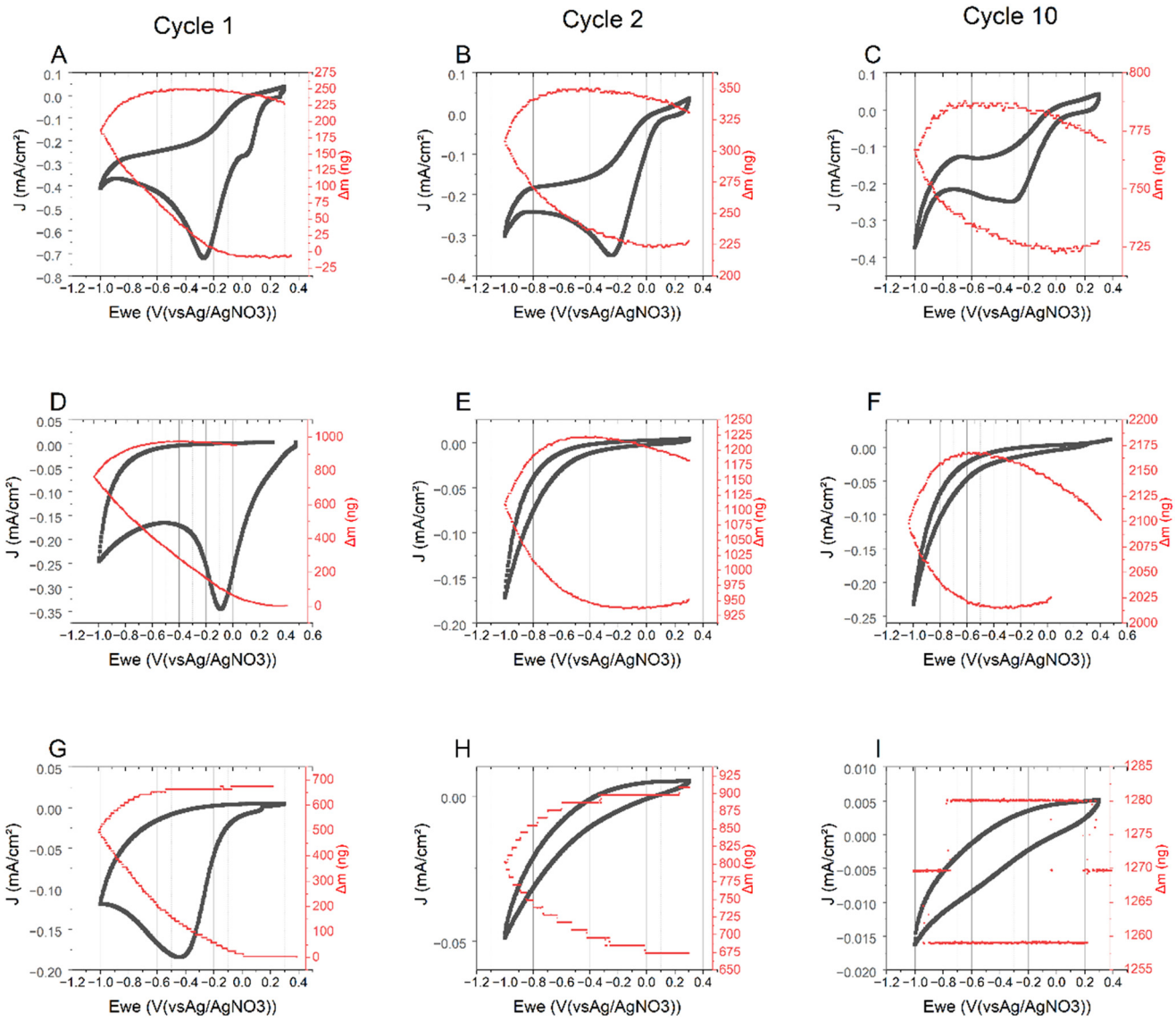

Fig. 7 Mass change and CV of the gold-quartz electrode for cycle 1, 2 and 10 for **DS_2(CF3)** (A–C), **DS_F4** (D–F) and **DS_C8F17** (G–I). All curves were recorded in acetonitrile (AN) with 0.1 M nBu$_4$PF$_6$ at a scan rate of 50 mV s^{-1} over 10 cycles between [−1 V; Eoc] *versus* Ag/Ag$^+$.

salt (black curve) demonstrates a halt in material deposition after the third cycle, with a mass gain of 24 μg cm^{-2}: the film becomes fully passivating. Finally, with **DS_2(CF3)** (red curve), the mass gain (15.8 μg cm^{-2}) is significantly lower as well as the increase in mass in the first cycle.

Fig. 7 plot the current density and mass change as a function of potential at three different stages of the grafting process (the 1st, 2nd and 10th cycles) and for the three considered salts (**DS_2(CF3)**, **DS_F4**, **DS_C8F17**). Compare to **DS_C8F17** which show only an increase in weight, the **DS_F4** and **DS_2(CF3)** curves present a gain and then a loss of material with each cycle. For these two last salts, the mass loss begins at −0.4 V *vs.* Ag/Ag$^+$. The observed mass gain can be attributed to a combination of chemisorbed and physisorbed film, while the mass loss can be explained by the desorption of organic compounds and the cations present inside the thin film in response to the applied potential. Indeed, it is evident that physisorbed species can be more readily removed from the surface than covalently grafted ones. Similar observations were reported by K. Daasbjerg *et al.*:[25] the increase in film mass during the forward scan toward the reduction potential was attributed to the irreversible attachment of diazonium species and the incorporation of electrolyte ions (Bu_4N^+) into the film. During the reverse scan, the observed decrease in mass was ascribed to the expulsion of ions and physisorbed species. Thus, these experiments demonstrates that cyclic voltammetry technique is able to remove some physisorbed species and let some place for the next cycle to able the reduction of new diazonium salt at the surface. Thus, the physisorption-desorption process explains the shape of the Fig. 4B and C, as well as the curves displayed in Fig. 5

Table 2 Grafting efficiency calculated from the integration of the CV reduction peak and the amount of material deposited (EQCM) after 1 cycle

Au/EQCM – cycle1		DS_F4	DS_C8F17	DS_246(F3)	DS_2(CF3)	DS_345(F3)
CV	$\lvert Q_{1CV}\rvert/S$ (mC cm^{-2})	35.0	9.5	5.5	13.5	25.0
EQCM	Γ (mol cm^{-2})	32.0×10^{-9}	7.0×10^{-9}	2.6×10^{-9}	0.2×10^{-9}	2.9×10^{-9}
	$\lvert Q_{1mass}\rvert/S$ (mC cm^{-2})	3.0	0.7	0.3	0.02	0.3
Grafting efficiency ($\lvert Q_{1mass}\rvert/\lvert Q_{1CV}\rvert$)		8.7%	7.4%	4.6%	0.1%	1.1%

based on sterically hindered diazonium salts. In contrast, for **DS_C8F17** (Fig. 7A–C), which enables the rapid creation of a highly passivating film with very low current density, no mass loss is observed. The film formed during the first three cycles directly allows complete surface passivation, preventing the formation of a physisorbed film.

By integrating the reduction peaks in the cyclic voltammetry of diazonium salt grafting on gold electrodes, the total charge passed was determined. EQCM also allows to estimate the number of moles deposited during one or multiple cycles. Consequently, the grafting density Γ (mol cm^{-2}) can be determined using the eqn (2):

$$\Gamma = \frac{Q}{n \cdot F \cdot S} \quad (2)$$

n is the number of electrons exchanged per grafted molecule (n = 1 here), Q is the charge transferred during the grafting reaction (C), F is the Faraday constant (96 485 C mol^{-1}), and S is the electroactive surface area (cm^2). From eqn (2) we quantify the charge involved in the grafting process as reported in Table 2.

First, the area under the reduction peak in the first cycle of the CV corresponds to the charge transferred during the reduction process. This charge quantity was compared to the charge needed to graft the mass of fluorinated compounds on the electrode to determine the grafting efficiency (Table 2). As expected, due to its free *para* position and lack of bulky substituents, the highest grafting efficiency was observed for **DS_F4** (8.7%), followed by **DS_C8F17** (7.4%) and **DS_246(F3)** (4.6%). In contrast, only 0.1% was obtained for **DS_2(CF3)** and 1.1% for **DS_345(F3)**, confirming the complexity of grafting these molecules. However, despite a very large difference in grafting efficiency, **DS_345(F3)** gained almost the same amount of mass as **DS_246(F3)**, which was less than **DS_C8F17** and **DS_F4** but greater than **DS_2(CF3)**.

The same analysis was then applied after 10 cycles (Table 3). Grafting efficiency remained nearly identical. The highest grafting density is observed for **DS_F4**, with 9.0×10^{-8} mol cm^{-2} and followed by **DS_C8F17** with 1.3×10^{-8} mol cm^{-2}.

Finally, the charge transfer during the 10th cycle was studied. It decreased compared to the first cycle for all molecules and was zero for **DS_C8F17**, demonstrating total electrode passivation. In contrast, **DS_F4** still exhibited a significant charge transfer (−6.5 mC cm^{-2}), indicating continuous grafting over the 10 cycles.

The mass gain evolution between the 1st and the 10th CV cycle ($\lvert Q_{1mass}\rvert/\lvert Q_{1–10mass}\rvert$) is consistent with the corresponding charge transfer ($\lvert Q_{1–10CV}\rvert/\lvert Q_{1CV}\rvert$). The mass increases by a factor of 3 for **DS_F4**, 1.8 for **DS_C8F17**, and 1.6 for **DS_246(F3)**. Hence, most of the molecules are grafted during the first cycle. For **DS_2(CF3)**, a mass gain factor of 10 is measured compared to a factor of 3 for charge transfer, indicating that the grafting process was not constant and was more efficient over successive cycle. Finally, **DS_345(F3)** shows a slight decrease in deposited material at after 10 cycles compared to the first cycle, while a factor of 1.6 is found for charge transfer. This could suggest the loss of a physisorbed layer.

Simultaneously, the ratios of the maximum reduction peak intensities (output from Fig. 2 and 4) of the second and first cycles are presented in last columns of Table 1. Assuming that the layer starts to form during the first cycle, the current difference provides an indication of the blocking effect of the layer formed during the first scan. The peak ratios on gold electrode for **DS_F4**, **DS_246(F3)**, and **DS_C8F17** on the gold electrode are 0.06, 0.03, and 0.06, respectively, clearly indicating the fastest-grafting diazonium salts. But, only **DS_C8F17** achieves almost total passivation after the second cycle. In contrast, **DS_345(F3)** and **DS_2(CF3)** exhibit ratios of 0.92 and 0.48, respectively, demonstrating the complexity of their grafting process, as confirmed by EQCM analyses. **DS_345(F3)** is more challenging to graft than **DS_F4**, likely due to the cleavage of a C–F bond, which supported by the formation of a passivating layer (Fig. 3). **DS_2(CF3)**, on the other hand, exhibits inefficient grafting, attributed to the spherical steric hindrance of its substituent,

Table 3 Grafting efficiency calculated from the integration of the CV reduction peak and the amount of material deposited (EQCM) after 10 cycle

Au/EQCM – cycle1–10		DS_F4	DS_C8F17	DS_246(F3)	DS_2(CF3)	DS_345(F3)
CV	$\lvert Q_{1–10CV}\rvert/S$ (mC cm^{-2})	101.7	16.3	9.0	40.9	39.1
EQCM	Γ (mol cm^{-2})	90.0×10^{-9}	13.0×10^{-9}	4.0×10^{-9}	2.2×10^{-9}	2.5×10^{-9}
	$\lvert Q_{1–10mass}\rvert/S$ (mC cm^{-2})	8.7	1.2	0.4	0.2	0.2
Grafting efficiency ($\lvert Q_{1–10mass}\rvert/\lvert Q_{1–10CV}\rvert$)		8.5%	7.4%	4.2%	0.5%	0.6%
$CV_{cycle10}$	$\lvert Q_{10CV}\rvert/S$ (mC cm^{-2})	6.5	0.0	0.3	4.0	0.7

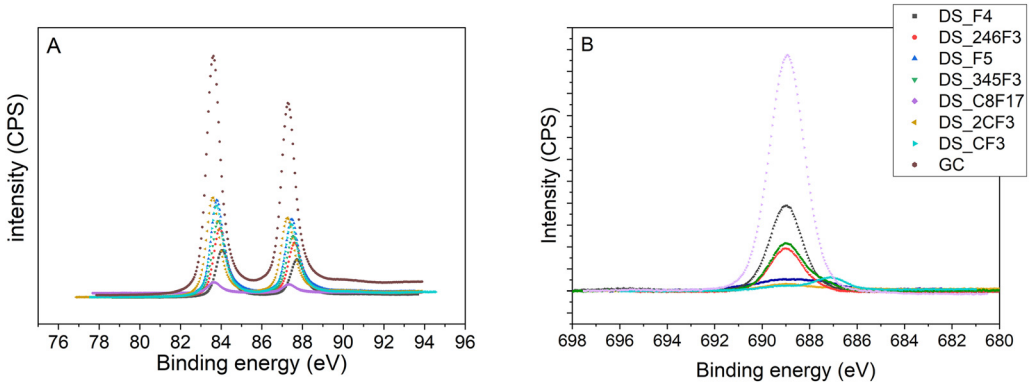

Fig. 8 (A) Au_{4f} and (B) F_{1s} core level spectra of Au thin film before and after modification by electrochemical reduction with various aryldiazonium salts.

which inhibits multilayer formation. The same trend is observed on the GC electrode. However, direct comparisons of key parameters—such as reduction potential, current density, and peak ratio of Table 1—between gold and GC surfaces are not meaningful due to the inherent differences in their surface properties. This observation aligns with previous studies, including that of Daasbjerg *et al.*,[25] who also reported difficulty in establishing a clear correlation between substrate type and film thickness or quality.

Chemical composition of grafted species on the gold surfaces were studied by XPS measurements. For this study, the salts were electrografted on gold on glass using cyclic voltammetry (10 cycles) from 0.3 to −1.0 V *vs.* Ag/Ag^+ reference electrode. Fig. 8 and Table 4 present the different XPS spectra and the composition of the electrodes, respectively, after their modification by electrochemical reduction with various aryldiazonium salts.

Survey spectra (ESI,† Fig. S6–S8) show for all grafting the presence of C_{1s} (284.9–295.2 eV), fluorine F_{1s} (689.0 eV for C–F bond) and gold Au_{4f} (84.0 and 87.8 eV). For some sample, a small amount of nitrogen is also observed, is assigned to azo bonds present inside the film. Hence, the chemical composition of grafted species confirm the presence of a fluorinated layer. No phosphorus peak is observed, indicating that the PF_6^- anions from the electrolyte are not present in the thin film. For **DS_CF3**, a boron peak (centered at 194.3 eV) and a fluorine peak (centered at 687.1 eV) highlight the presence of BF_4^- anion, the counterion associated with the diazonium salt.

Fig. 8A and B presents the Au_{4f} and F_{1s} core-level XPS spectra, respectively. The intensity of the Au_{4f} and F_{1s} peaks varies depending on the grafting. Table 4 details the composition of electrodes after the grafting with the different aryldiazonium salts. Atomic composition of each element was obtained classically by the integration of the XPS signal. Peak areas were corrected by taking into account the Scofield sensitivity factors (1.00 for C, 17.12 for Au and 4.43 for F). We observe a decrease in the percentage of gold surface component after its electrochemical functionalization with **DS_2(CF3)** (65.42 at%), **DS_CF3** (61.37 at%), **DS_F5** (61.28 at%) **DS_345(F3)** (32.62 at%), **DS_246(F3)** (16.26 at%), **DS_F4** (11.73 at%) and **DS_C8F17** (4.92 at%). The use of a long-chain salt such as **DS_C8F17** significantly inhibits the intensity of both Au_{4f} peaks. Diazonium salts with hydrogen in *para* or *meta* positions are also relatively efficient. In contrast, the gold substrate modified with **DS_F5**, **DS_CF3** and **DS_2(CF3)** exhibits high-intensity gold peaks, although it is lower than that of the reference electrode.

The F_{1s} peak intensity is notably higher for **DS_C8F17** compared to the other diazonium salts, reflecting the greater number of fluorine atoms in the substituent: **DS_C8F17** (48.03 at%) > **DS_F4** (20.46 at%) > **DS_2(CF3)** (3.55 at%) > **DS_246(F3)** (11.51 at%). However, normalizing the atomic composition of fluorine based on the number of fluorine atoms in each substituent (last column of Table 4) reveals that **DS_F4** is the most abundant diazonium salt grafted on the surface. In contrast, **DS_2(CF3)** and **DS_CF3** are the least represented substituents, further confirming the hypothesis

Table 4 Atomic composition (at%) after the grafting with the seven studied aryldiazonium salts: **DS_C8F17**, **DS_F4**, **DS_246(F3)**, **DS_345(F3)**, **DS_F5**, **DS_CF3**, **DS_2(CF3)**

	Au (% at)	C (% at)	F (% at)	Number of F	F normalized (% at)
DS_C8F17	4.92	47.05	48.03	17	2.83
DS_F4	11.73	67.81	20.46	4	5.12
DS_246(F3)	16.26	72.23	11.51	3	3.84
DS_345(F3)	32.62	53.41	13.98	3	4.66
DS_F5	61.28	31.48	7.24	5	1.45
DS_CF3	61.37	32.38	6.25	3	2.08
DS_2(CF3)	65.42	31.03	3.55	6	0.59

regarding the complexities involved in its grafting (Fig. 4). Finally, as previously mentioned, **DS_C8F17**, despite not having the highest number of grafted molecules, owes its surface prevalence to the length of its chain, enabling the formation of a compact passivating film. These observations can be explained by the fact that **DS_C8F17** creates a continuous passivating film using fewer layers of diazonium salts compared to **DS_F4**, which has a geometry that favors the formation of a multilayer only in *para* position. Finally, **DS_345(F3)** and **DS_F5** contain a large number of fluorine atoms (13.98 at% and 7.24 at%), which confirm the release of fluorine and the formation of multilayer thin film.

Finally, the detection of gold can be explained either by the formation of a film thinner than the 10 nm analysis depth of XPS[26] or the presence of hole in the electrografted films. To verify the homogeneity of the films, the response of diazonium salts grafted onto a gold electrode was tested in $Fe(CN)_6^{3-/4-}$ solution in an aqueous electrolyte. If the film is homogeneous, no Ferri/Ferro redox system should be observed, in contrast to a pinhole thin film.

Influence of steric effect and chain length on the post-grafting property: barrier effect and hydrophobicity

The cyclic voltammogram of soluble electroactive species provides a convenient tool to study the presence of grafted film and their passivation properties. The influence on the CV response of $Fe(CN)_6^{3-/4-}$ oxido-reduction was investigated for different organic layers grafted by Cyclic voltammetry (10 cycles). The voltammogram of the $Fe(CN)_6^{3-/4-}$ redox system present a quasi-reversible behavior at the bare electrode with an apparent redox potential of 0.23 V *vs.* Ag/AgCl. Fig. 9 shows the CV curves recorded following the grafting process of the different diazonium salts, compared to the bare gold electrode used as a reference. A magnified view is shown in Fig. 9B to allow clearer distinction between the curves. After grafting with **DS_C8F17**, **DS_F4**, **DS_246(F3)**, and **DS_345(F3)**, the electrodes exhibit significant blocking behavior of oxidation and reduction reactions as the CV is flat near zero. The deposited layer is therefore homogeneous. In contrast, after grafting with **DS_CF3**, **DS_2(CF3)**, and **DS_F5**, electrodes exhibit a $Fe(CN)_6^{3-/4-}$ redox peaks, indicating that the deposited layer is not homogeneously formed on the surface. However, the fluorine directly attached on the aromatic ring is more efficient than trifluromethyl groups. As summary, the ranking of the molecules in decreasing order of efficient for forming a continuous passivating layer on gold is: **DS_C8F17** > **DS_F4** > **DS_246(F3)** > **DS_345(F3)** > **DS_F5** > **DS_2(CF3)** > **DS_CF3**.

The same test was performed on a GC electrode (Fig. S9†). We found that all salts achieve a continuous uniform passivating layer. This difference is attributed to the easier grafting process on carbon surfaces with the formation of a C–C bond compared to gold surfaces with a C–Au Bond.

Finally, contact angle measurements were performed on all electrodes after grafting process. To ensure a flat measurement surface from the commercial electrodes, a custom 3D-printed holder was fabricated (see ESI,† Fig. S10). A 2 μL water droplet was deposited on the surface and analyzed using the SCA20 software. These measurements served as an indicator of the successful modification of the surface, providing a straightforward method to evaluate the effectiveness and consistency of the grafting procedure. At first, the contact angles obtained on bare GC and gold were 57.7° and 33°, respectively. After grafting, the contact angles of all surfaces (GC and Au electrode) increase (Table S1†), confirming the more hydrophobic behavior and the successful surface modification. Fluorinated groups are well known for enhancing surface hydrophobicity due to their low surface energy and water-repellent properties.[27] However, the **DS_246(F3)** and **DS_F4** salts, which have a high grafting efficiency, show the lowest contact angle, with some values lower than 90°. Compounds with lower grafting efficiency give higher contact angles, which can be explained by the

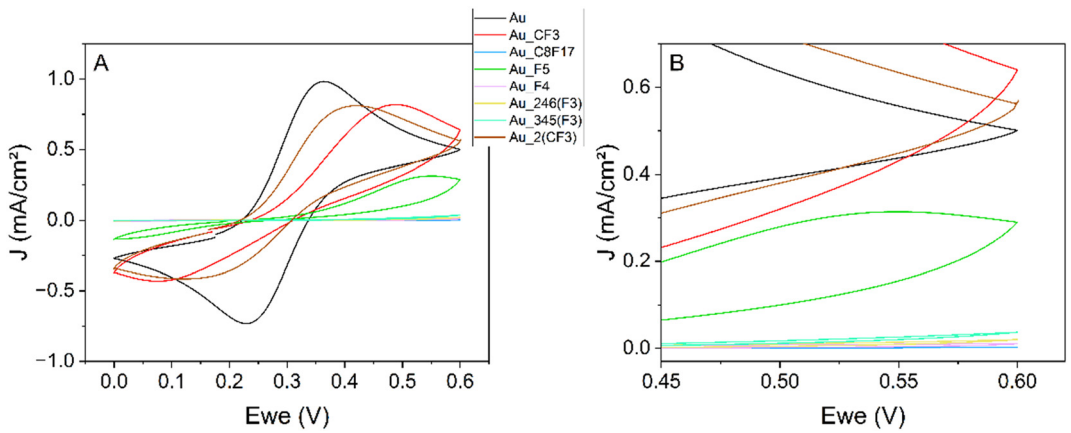

Fig. 9 (A) Cyclic voltammograms at a scan rate of 50 mV s^{-1} for gold electrodes in a 5 mM $Fe(CN)_6^{3-/4-}$ solution before and after deposition of different diazonium salts: **DS_CF3** (red); **DS_C8F17** (blue); **DS_F5** (green); **DS_F4** (pink); **DS_246(F3)** (orange); **DS_345(F3)** (cyan); and **DS_2(CF3)** (brown) and (B) it zoom.

Table 5 Surface energy of glassy carbon (GC) and gold electrodes after grafting with **DS_C8F17**, **DS_2(CF3)**, and **DS_F4**

	DS_C8F17		DS_2(CF3)		DS_F4	
Surface	GC	Au	GC	Au	GC	Au
Surface energy (mJ m^{-2})	19.5	18.3	23.2	25.0	27.7	27.2

roughness of the electrografted samples. Finally, two compounds (**DS_2(CF3)** and **DS_C8F17**) have some contact angles over 100° thanks to their fluorinated alkyl chain.

Surface tension values (in mJ m^{-2}) were calculated for two compounds (**DS_C8F17** and **DS_2(CF3)**) which exhibited high contact angles with water, and one compound (**DS_F4**) with a comparatively low contact angle. Surface energy was determined using the Owens–Wendt model.[28] Contact angles were measured using three probe liquids—water, ethanol, and squalene (a non-polar solvent)[28–30]—on the grafted surfaces. These measurements, along with the known surface energy values of the solvents, were used to construct Owens–Wendt plots (Table S2†). The complete methodology is provided in the ESI.†

The surface energy values of the grafted surfaces are summarized in Table 5. A surface energy $\gamma < 20$ mJ m^{-2} indicates a highly hydrophobic surface, while values between 20 and 35 mJ m^{-2} correspond to a hydrophobic surface.[31] In the study, surface energy decreases from **DS_F4** (27.7 on GC and 27.2 mJ m^{-2} on Au), to **DS_2(CF3)** (23.2 on GC and 25.0 mJ m^{-2} on Au), both of which display hydrophobic behavior. In contrast, **DS_C8F17** exhibits significantly lower surface energy value (19.5 on GC and 18.3 mJ m^{-2} on Au) indicating a highly hydrophobic surface ($\gamma < 20$ mJ m^{-2}). For reference, polytetrafluoroethylene (PTFE or Teflon) has a surface energy between 17.5 and 20.5 mJ m^{-2}.[31,32] These results show that an electrografted thin film of just a few nanometers of **DS_C8F17** can impart surface properties comparable to those of Teflon.

4. Conclusion

In summary, seven fluorinated diazonium salts were synthesized and positively grafted onto gold and carbon electrodes. The chemical structure proved to be a key factor influencing the mechanism of growth, on the surface roughness, on the passivation and on the hydrophobicity. Indeed, two different grafting behavior were observed depending on diazonium salts. **DS_C8F17**, **DS_F4**, and **DS_246(F3)** salts exhibit a high grafting efficiency (between 4.6% and 8.7%) associated with a low current density on the first CV cycle and the creation of a continuous passivating thin film. In contrast, **DS_345(F3)**, **DS_F5**, **DS_CF3** and **DS_2(CF3)** salts require the formation of a significant number of radicals (high current density on the CVs) to be grafted onto Au and GC electrodes. As proved by the experiments of the ultrasonic treatment and surface passivation which cannot be achieved with a monolayer, the **DS_345(F3)** and **DS_F5** salts are well chemisorbed on the surface, thus breaking a C–F bond to create multilayer. **DS_CF3** and **DS_2(CF3)** salts, containing trifluoromethyl groups, are the most difficult thin film to form due to the steric effect. As demonstrated for methyl substituents on diazonium salts, these two compounds will be able to go close to monolayer. Physisorbed species were also formed during the electrochemical grafting process, but were removed from the electrode in the forward cycle as indicated by the EQCM experiments. This explains why the difference in potential does not play a role and the shape of the curves obtained by cyclic voltammetry. **DS_C8F17** is the only compound that offers total passivation after 3 cycles without forming physisorbed species. It also has the most hydrophobic surface. In addition, **DS_F4** and **DS_246(F3)** were found to be effective passivation, in contrast to **DS_CF3** and **DS_2(CF3)** which present a high surface hydrophobicity thanks to the film's roughness.

This work demonstrates the feasibility of producing thin (<10 nm), hydrophobic, and covalently grafted films that are stable under ultrasonic treatment. The successful electrochemical grafting of fluorinated diazonium salts offers a promising strategy to reduce the amount of PFAS required for surface modification.

Data availability

• The data supporting this article have been included as part of the ESI.†

• All data for this article, including electrochemistry, NMR, IR, XPS, EQCM are available at **http://doi.org/10.5281/zenodo.15211416**.

Conflicts of interest

There are no conflicts to declare.

Acknowledgements

The authors acknowledge the HIPOHYBAT project, funded by the "France 2030" government investment plan managed by the French National Research Agency, under the reference "ANR-22-PEBA-0003".

References

1 **https://www.efpia.eu/media/52ipvgfi/annex-1-efpia_sea_pfas_final.pdf**, (accessed 9 April 2025).
2 M. G. Evich, M. J. B. Davis, J. P. McCord, B. Acrey, J. A. Awkerman, D. R. U. Knappe, A. B. Lindstrom, T. F. Speth, C. Tebes-Stevens, M. J. Strynar, Z. Wang, E. J. Weber, W. M. Henderson and J. W. Washington, *Science*, 2022, **375**, eabg9065.
3 S. Y. Wee and A. Z. Aris, *Ecotoxicol. Environ. Saf.*, 2023, **267**, 115663.
4 H. Brunn, G. Arnold, W. Körner, G. Rippen, K. G. Steinhäuser and I. Valentin, *Environ. Sci. Eur.*, 2023, **35**, 20.

5 A. Perrotta, P. Christian, A. O. F. Jones, F. Muralter and A. M. Coclite, *Macromolecules*, 2018, **51**, 5694–5703.
6 G.-R. Choi, J. Park, J.-W. Ha, W.-D. Kim and H. Lim, *Macromol. Mater. Eng.*, 2010, **295**, 995–1002.
7 J. H. Yim, *Surf. Coat. Technol.*, 2013, **234**, 21–32.
8 K. Ellinas, A. Tserepi and E. Gogolides, *Langmuir*, 2011, **27**, 3960–3969.
9 A. J. Downard, *Electroanalysis*, 2000, **12**, 1085–1096.
10 V. Mévellec, S. Roussel, L. Tessier, J. Chancolon, M. Mayne-L'Hermite, G. Deniau, P. Viel and S. Palacin, *Chem. Mater.*, 2007, **19**, 6323–6330.
11 S. Baranton and D. Bélanger, *J. Phys. Chem. B*, 2005, **109**, 24401–24410.
12 L. Pichereau, I. López, M. Cesbron, S. Dabos-Seignon, C. Gautier and T. Breton, *Chem. Commun.*, 2019, **55**, 455–457.
13 H. Casademont, L. Fillaud, X. Lefèvre, B. Jousselme and V. Derycke, *J. Phys. Chem. C*, 2016, **120**, 9506–9510.
14 L. T. Nielsen, K. H. Vase, M. Dong, F. Besenbacher, S. U. Pedersen and K. Daasbjerg, *J. Am. Chem. Soc.*, 2007, **129**, 1888–1889.
15 Z. Peng, A. H. Holm, L. T. Nielsen, S. U. Pedersen and K. Daasbjerg, *Chem. Mater.*, 2008, **20**, 6068–6075.
16 C. Combellas, D. Jiang, F. Kanoufi, J. Pinson and F. I. Podvorica, *Langmuir*, 2009, **25**, 286–293.
17 T. Menanteau, E. Levillain and T. Breton, *Chem. Mater.*, 2013, **25**, 2905–2909.
18 J. Pinson and F. Podvorica, *Chem. Soc. Rev.*, 2005, **34**, 429.
19 J. Billon, V. Shkirskiy, S. Dabos-Seignon, T. Breton and C. Gautier, *Phys. Chem. Chem. Phys.*, 2022, **24**, 14294–14298.
20 M. Tanaka, T. Sawaguchi, Y. Sato, K. Yoshioka and O. Niwa, *Langmuir*, 2011, **27**, 170–178.
21 A. Benedetto, M. Balog, P. Viel, F. Le Derf, M. Sallé and S. Palacin, *Electrochim. Acta*, 2008, **53**, 7117–7122.
22 A. Barfidokht, S. Ciampi, E. Luais, N. Darwish and J. J. Gooding, *Anal. Chem.*, 2013, **85**, 1073–1080.
23 M. Cesbron, Vers l'élaboration de surfaces modifiées par des monocouches organiques mixtes issues de la réduction de précurseurs diazonium, *These de doctorat*, Université d'Angers, Angers, 2019, **https://theses.fr**, **https://theses.fr/2019ANGE0061**.
24 W.-Y. Tsai, P.-L. Taberna and P. Simon, *J. Am. Chem. Soc.*, 2014, **136**, 8722–8728.
25 S. Chernyy, A. Bousquet, K. Torbensen, J. Iruthayaraj, M. Ceccato, S. U. Pedersen and K. Daasbjerg, *Langmuir*, 2012, **28**, 9573–9582.
26 D. N. G. Krishna and J. Philip, *Appl. Surf. Sci. Adv.*, 2022, **12**, 100332.
27 J.-D. Brassard, D. K. Sarkar and J. Perron, *Appl. Sci.*, 2012, **2**, 453–464.
28 D. K. Owens and R. C. Wendt, *J. Appl. Polym. Sci.*, 1969, **13**, 1741–1747.
29 F. M. Fowkes, F. L. Riddle, W. E. Pastore and A. A. Weber, *Colloids Surf.*, 1990, **43**, 367–387.
30 F. A. M. M. Gonçalves, A. R. Trindade, C. S. M. F. Costa, J. C. S. Bernardo, I. Johnson, I. M. A. Fonseca and A. G. M. Ferreira, *J. Chem. Thermodyn.*, 2010, **42**, 1039–1049.
31 H. W. Fox and W. A. Zisman, *J. Colloid Sci.*, 1950, **5**, 514–531.
32 A. C. Zettlemoyer, *J. Colloid Interface Sci.*, 1968, **28**, 343–369.